HUBBARD MODEL

The Wiedemann-Franz law in doped Mott insulators without quasiparticles

Wen O. Wang[1,2]*, Jixun K. Ding[1,2], Yoni Schattner[2,3,4], Edwin W. Huang[5,6,7], Brian Moritz[2], Thomas P. Devereaux[2,8,9]*

Many metallic quantum materials display anomalous transport phenomena that defy a Fermi liquid description. Here, we use numerical methods to calculate thermal and charge transport in the doped Hubbard model and observe a crossover separating high- and low-temperature behaviors. Distinct from the behavior at high temperatures, the Lorenz number L becomes weakly doping dependent and less sensitive to parameters at low temperatures. At the lowest numerically accessible temperatures, L roughly approaches the Wiedemann-Franz constant L_0, even in a doped Mott insulator that lacks well-defined quasiparticles. Decomposing the energy current operator indicates a compensation between kinetic and potential contributions, which may help to clarify the interpretation of transport experiments beyond Boltzmann theory in strongly correlated metals.

Landau's notion of quasiparticles greatly simplified the language of transport in systems with a macroscopic number of interacting degrees of freedom in terms of "free" objects with renormalized properties that participate in transport through a semi-classical or Boltzmann framework. As such, transport behavior of Fermi liquids is governed solely by kinematic constraints of a Fermi surface and collisions between otherwise free particles. Yet in many correlated metals, including the high–transition temperature (or critical temperature, T_c) cuprates, anomalous transport phenomena have been uncovered that violate these rules: strange metal resistivity that increases linearly with temperature, not saturating as the quasiparticle mean-free-path approaches the lattice spacing (*1*–*3*); inconsistency with Kohler's rule, which governs the scaling behavior of magnetoresistance from Boltzmann theory (*4*–*6*); and violations of the Wiedemann-Franz law, which constrains the ratio of thermal to electrical conductivity (*7*–*18*).

The ubiquity of behavior that violates notions of the Fermi liquid has led to tremendous interest in determining how heat and charge currents propagate in such systems (*19*–*23*). Analysis of the large body of experimental transport results in correlated materials has been hindered by the use of an assumed Boltzmann-like theory and reductive conclusions on the nature of transport in terms of Drude-like single-particle concepts. This greatly amplifies the need for deeper analysis that avoids oversimplifications, but there is very little known from exact methods about the nature of transport in strongly interacting systems. Many advanced numerical calculations have focused on characterizing ground-state properties (*24*, *25*), but a picture of transport is incomplete without an understanding of the excited states in these materials. Analytical approaches are hampered by the fact that properly evaluating transport involves calculating many higher-order correlation functions without relying on the simplifying assumptions of quasiparticles and Boltzmann theory, which only punctuates the need for more accurate and precise determinations of transport.

Here, we numerically study the DC longitudinal thermal conductivity κ in the doped two-dimensional (2D) $t-t'-U$ Hubbard model, which exhibits strange metallic electric transport over a wide hole doping p and temperature T range (*26*–*29*). We evaluate the many-body Kubo formula using the determinant quantum Monte Carlo (DQMC) (*30*, *31*) algorithm, which is numerically exact, unbiased, and nonperturbative, and maximum entropy analytic continuation (MaxEnt) (*32*, *33*), which is typically reliable in systems with strong interactions that lack sharp features in frequency [see supplementary materials of (*26*)].

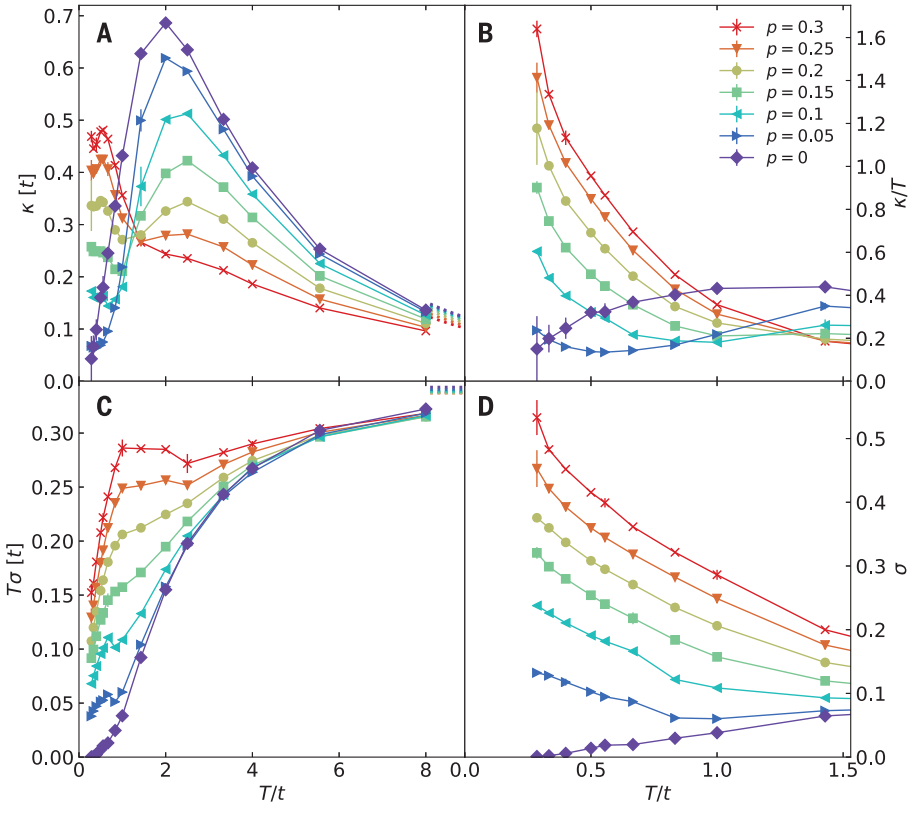

Fig. 1. Temperature and doping dependence of thermal and charge conductivity. (**A**) DC thermal conductivity κ. (**B**) κ/T focused on the low-temperature regime. (**C**) DC charge conductivity σ multiplied by temperature T. (**D**) σ focused on the low-temperature regime. The high-temperature dotted lines in (A) and (C) are infinite-temperature limits calculated via a moments expansion (*26*, *35*). Parameters: $U/t = 8$ and $t'/t = -0.25$. A crossover temperature $T_{x0} \sim t$ separates low- and high-temperature regimes in (A) and (C). Error bars are shown but may be smaller than the size of the data markers.

[1]Department of Applied Physics, Stanford University, Stanford, CA 94305, USA. [2]Stanford Institute for Materials and Energy Sciences, SLAC National Accelerator Laboratory, 2575 Sand Hill Road, Menlo Park, CA 94025, USA. [3]Department of Physics, Stanford University, Stanford, CA 94305, USA. [4]AWS Center for Quantum Computing, Pasadena, CA 91125, USA. [5]Department of Physics and Institute of Condensed Matter Theory, University of Illinois at Urbana-Champaign, Urbana, IL 61801, USA. [6]Department of Physics and Astronomy, University of Notre Dame, Notre Dame, IN 46556, USA. [7]Stavropoulos Center for Complex Quantum Matter, University of Notre Dame, Notre Dame, IN 46556, USA. [8]Department of Materials Science and Engineering, Stanford University, Stanford, CA 94305, USA. [9]Geballe Laboratory for Advanced Materials, Stanford University, Stanford, CA 94305, USA.
*Corresponding author. Email: wenwang.physics@gmail.com (W.O.W.); tpd@stanford.edu (T.P.D.)

We define κ as the linear response of the heat current $\langle \mathbf{J}_Q \rangle$ induced by a parallel temperature gradient and normalized by system size N, $\kappa \equiv -\langle J_{Q,x} \rangle / (N \partial_x T)$, under the condition of zero charge current. Distinct from the incoherent behavior at high temperatures, we observe that the Lorenz number, the ratio between the thermal and charge conductivity $L \equiv \kappa/(T\sigma)$, has a weak doping and parameter dependence in the low-temperature regime and roughly approaches the Wiedemann-Franz law prediction $L_0 = \pi^2/3$ as temperature decreases down to the lowest accessible value, even in the absence of long-lived quasiparticles. Methodological details, including a systematic analysis of finite size and Trotter errors, as well as extensive supporting data, can be found in (*34*).

Thermal and charge conductivity

The DC longitudinal thermal conductivity $\kappa(T)$ is shown in Fig. 1A; for comparison, the DC longitudinal charge conductivity $\sigma(T)$ (*26*) (multiplied by T) is shown in Fig. 1C. In the infinite-temperature limit, $\kappa \propto 1/T^2$ and $\sigma \propto 1/T$ (*26*, *27*, *35*, *36*). As T decreases from this limit, we observe a crossover at roughly $T_{xo} \sim t$, separating distinct behavior in two regimes for both κ and σ. κ decreases with doping at high temperatures, whereas it increases with doping at low temperatures. Although σ generally increases with doping at all temperatures, the temperature dependence of $T\sigma$ displays kinks, or even nonmonotonic behavior, at roughly T_{xo}. Below T_{xo}, κ/T and σ display similar doping and temperature dependences (Fig. 1, B and D), suggesting persistent correlations between thermal and charge transport even for a strange metal phase where quasiparticles are not well-defined.

Lorenz number and its temperature and parameter dependence

The Lorenz number $L(T)$ highlights the correlation between thermal and charge transport (Fig. 2). Aside from the half-filled Mott insulator, where L diverges with decreasing temperature, in the doped metals L shows a crossover similar to that in κ and σ. At high temperatures, high-energy excited states become important (*36*, *37*), such that quasiparticles are not well-defined and electrons have extraordinarily short mean-free-paths. L has a nonmonotonic temperature dependence and decreases with increasing doping. Below T_{xo}, L displays substantially reduced doping dependence, collapsing roughly onto a single set of curves. This set of curves increases monotonically with decreasing temperatures, approaching a constant that roughly corresponds to $L_0 = \pi^2/3$—the Lorenz number as predicted by the Wiedemann-Franz law.

In the Hubbard model, relaxation primarily occurs through Umklapp scattering. To test its impact on the conductivities and L, we modulate Umklapp scattering by modifying

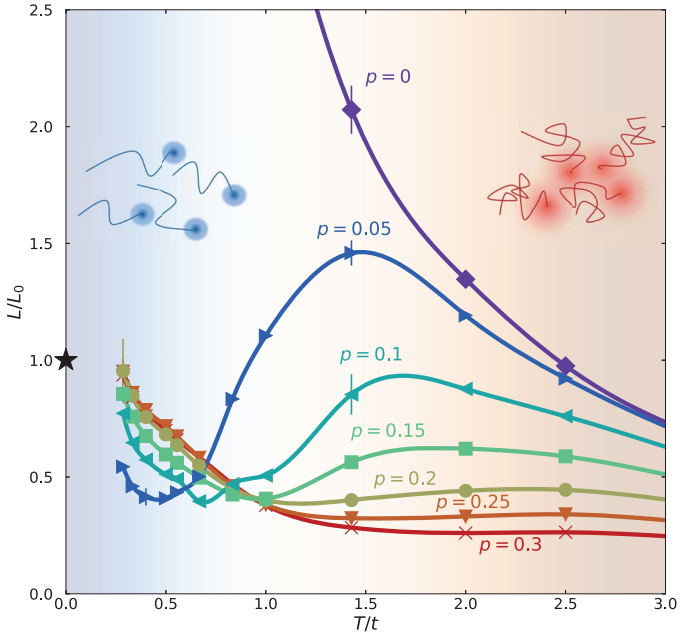

Fig. 2. Lorenz number. Symbols: Calculated $L = \kappa/(T\sigma)$ normalized by L_0. The lines are guides to the eye. At low temperatures, below $T_{xo} \sim t$, L/L_0 approaches roughly 1, marked by the black star. Parameters: $U/t = 8$ and $t'/t = -0.25$. Cartoons: At high temperatures, high-energy excited states are important (*36*, *37*) and transport is incoherent; electrons are strongly correlated and have an extraordinarily short mean-free-path. At low temperatures, the electrons are on their way toward some sort of "coherence"; electrons have a longer mean-free-path, although not long enough for well-defined long-lived quasiparticles. Although single-particle and individual transport properties show signatures of anomalous strange metal and non-Fermi liquid behavior, the Lorenz number still roughly approaches the Wiedemann-Franz law's prediction as temperature decreases.

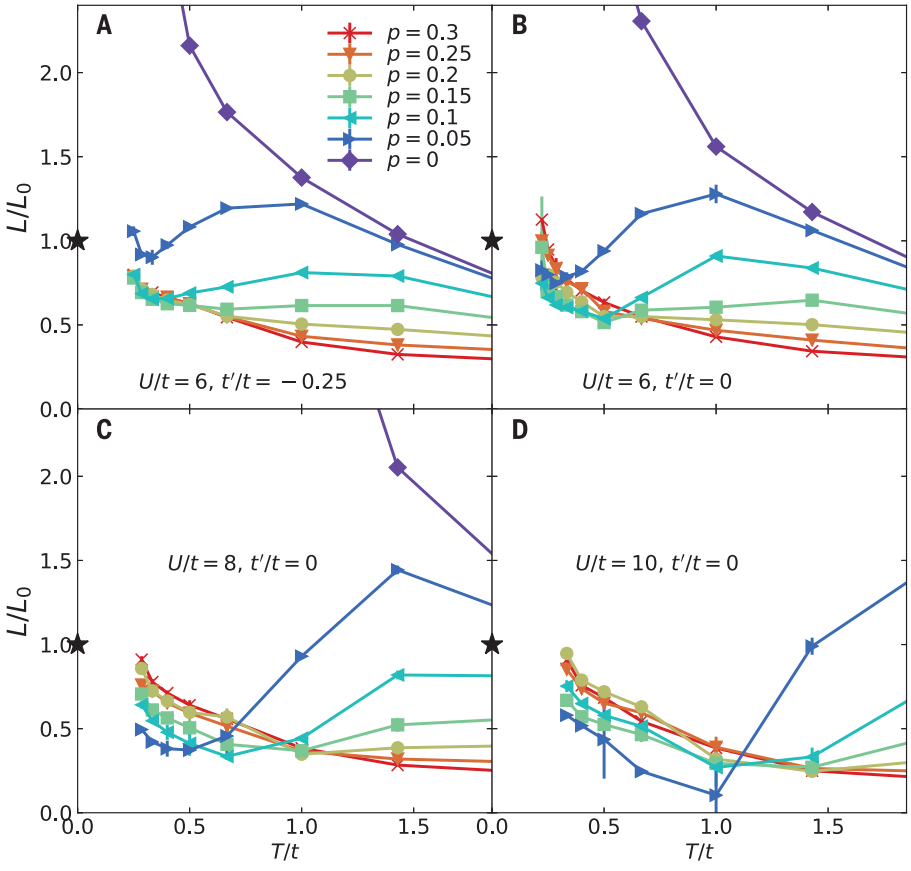

Fig. 3. Parameter dependence of the Lorenz number. L/L_0 for (**A**) $U/t = 6$ and $t'/t = -0.25$; (**B**) $U/t = 6$ and $t'/t = 0$; (**C**) $U/t = 8$ and $t'/t = 0$; (**D**) $U/t = 10$ and $t'/t = 0$. The black stars mark the value 1. The lowest temperatures are lower for smaller U owing to a better behaved fermion sign.

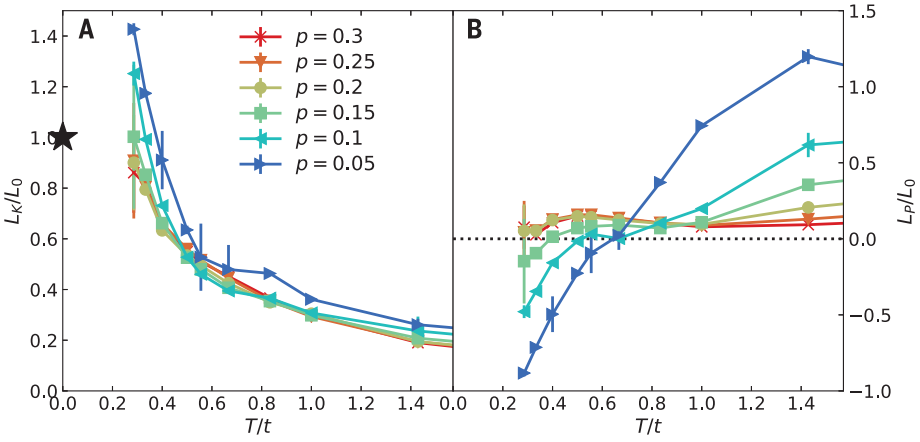

Fig. 4. Kinetic and potential decomposition of the Lorenz number. (**A**) Normalized kinetic contribution L_K/L_0. The black star marks the value 1. (**B**) Normalized potential contribution L_P/L_0. The black dotted line marks the value 0. Parameters: $U/t = 8$ and $t'/t = -0.25$.

the Hubbard U and next-nearest-neighbor hopping t', with the results shown in Fig. 3. The high-temperature peak position of L is largely controlled by U, increasing with increasing U, similar to the behavior of the specific heat [see fig. S9 in (*34*)]. For temperatures below the crossover, there is no strong dependence of L on either U or t', suggesting that the low-temperature behavior is generic to the strongly correlated Hubbard model: Changing the shape of the Fermi surface (t') or the strength of Umklapp scattering (U) does not appreciably alter L at the temperatures accessible through DQMC.

Decomposing the Lorenz number

To better understand the behavior below T_{xo}, it is useful to look at the operator contributions to the conductivities. Determining κ in the Hubbard model using the Kubo formula requires one to consider the two-particle term in the energy current operator arising from electron-electron interactions, as opposed to Boltzmann theory that relies entirely on single-particle properties. The energy current operator $\mathbf{J}_E$ consists of a single-particle kinetic energy contribution, $\mathbf{J}_K$, similar to that appearing in the charge current operator $\mathbf{J}$, plus an additional term $\mathbf{J}_P$, which we call the potential energy current that depends explicitly on the interaction and notably contains a two-particle current [see eq. S2, eq. S3, and the relevant discussion of the Formalism in (*34*)]. The heat current $\mathbf{J}_Q$, from which we obtain κ, itself contains an additional term $-\mu\mathbf{J}$, where μ is the chemical potential. However, under the condition of zero charge current ($\langle\mathbf{J}\rangle = 0$), terms proportional to $\langle\mathbf{J}\rangle$ will not contribute to $\langle\mathbf{J}_Q\rangle$, leaving only $\langle\mathbf{J}_K\rangle$ and $\langle\mathbf{J}_P\rangle$. In this way, we separate κ into kinetic and potential contributions $\kappa_{K/P} \equiv -\langle J_{K/P,x}\rangle/(N\partial_x T)$. Similarly, we can express the Lorenz number L as a sum of its kinetic and potential contributions, with $L = L_K + L_P$, where $L_{K/P} \equiv \kappa_{K/P}/(T\sigma)$ (Fig. 4, A and B).

At high temperatures, the kinetic energy contribution L_K is relatively small and doping independent, whereas the potential energy contribution L_P is large at small doping and decreases for increasing hole concentration owing to the reduction of double occupancies. This doping dependence is imparted to the combined L (as already shown in Fig. 2). Below the crossover temperature T_{xo} and at large doping, L_P is relatively small and L_K and L approach L_0. At low doping, L_K increases with decreasing temperature, while L_P decreases and changes sign at roughly T_{xo}. The separate contributions from the kinetic and potential terms show opposing behavior, which becomes more pronounced for lower doping, and effectively compensate one another, resulting in L that approaches L_0. Thus unexpectedly, the ratio L displays a relative insensitivity to doping, and Hubbard model parameters [see fig. S10 in (*34*)], at the lowest accessible temperatures.

Discussion and outlook

The congruence between charge and thermal transport in the Hubbard model is unexpected. For scattering dominated by elastic processes, such as disorder or quasi-elastic phonon scattering above the Debye temperature, the thermal and charge conductivity are correlated through the Wiedemann-Franz law (*13*, *21*, *38*, *39*), such that for T much lower than the Fermi temperature, one obtains the Lorenz number $L = L_0 = \pi^2/3$. For both Fermi liquids and non-Fermi liquids without disorder, L deviates substantially from L_0 (*21*, *39*, *40*). Despite our lack of knowledge about the exact behavior of the Hubbard model at lower temperatures (Fermi liquid or not), caused by the fermion sign problem, the result that L approaches a weakly doping and Hubbard parameter–dependent constant very close to L_0 indicates a surprisingly universal behavior. This behavior is observed only when both single- and two-particle contributions are properly accounted for in the heat-current operator.

Our results may be understood in three possible ways. First, although the temperatures in our study are below the magnetic exchange energy scale J, our results may not yet be in the asymptotic low-temperature regime to assess the $T \to 0$ limit. Second, one might expect the approximate Wiedemann-Franz ratio to emerge in a system where both charge and thermal currents relax predominantly through Umklapp scattering in our temperature regime. Lastly, it may be that such a compensation effect between kinetic and potential energy contributions to L cannot be cast in the usual Boltzmann-like formulation for strongly interacting, anisotropic systems such as the Hubbard model.

Finally, what can our results say about the strong violation of the Wiedemann-Franz law that has been observed in cuprates at room temperature, with L larger than L_0 by a factor of 3 or more (*7*, *10*, *18*, *38*)? One explanation for this is that the strong interaction enhances the electronic contribution to thermal transport, whereas another explanation would rely on a substantial phonon contribution to the heat current. Our observation over the experimentally relevant temperature range that the electronic contribution L roughly approaches L_0 from below would be consistent with scenarios in which the large L in cuprates requires an appreciable phonon contribution to heat transport.

REFERENCES AND NOTES

1. O. Gunnarsson, M. Calandra, J. E. Han, *Rev. Mod. Phys.* **75**, 1085–1099 (2003).
2. N. E. Hussey, K. Takenaka, H. Takagi, *Philos. Mag.* **84**, 2847–2864 (2004).
3. P. W. Phillips, N. E. Hussey, P. Abbamonte, *Science* **377**, eabh4273 (2022).
4. J. M. Harris *et al.*, *Phys. Rev. Lett.* **75**, 1391–1394 (1995).
5. J. Ayres *et al.*, *Nature* **595**, 661–666 (2021).
6. T. Kimura *et al.*, *Phys. Rev. B Condens. Matter* **53**, 8733–8742 (1996).
7. P. B. Allen, X. Du, L. Mihaly, L. Forro, *Phys. Rev. B Condens. Matter* **49**, 9073–9079 (1994).
8. R. W. Hill, C. Proust, L. Taillefer, P. Fournier, R. L. Greene, *Nature* **414**, 711–715 (2001).
9. C. Proust, E. Boaknin, R. W. Hill, L. Taillefer, A. P. Mackenzie, *Phys. Rev. Lett.* **89**, 147003 (2002).
10. H. Minami *et al.*, *Phys. Rev. B Condens. Matter* **68**, 220503 (2003).
11. S. Nakamae *et al.*, *Phys. Rev. B Condens. Matter* **68**, 100502 (2003).
12. C. Proust, K. Behnia, R. Bel, D. Maude, S. I. Vedeneev, *Phys. Rev. B Condens. Matter Mater. Phys.* **72**, 214511 (2005).
13. X. F. Sun *et al.*, *Phys. Rev. B Condens. Matter Mater. Phys.* **80**, 104510 (2009).
14. G. Grissonnanche *et al.*, *Phys. Rev. B* **93**, 064513 (2016).
15. J. Zhang *et al.*, *Proc. Natl. Acad. Sci. U.S.A.* **114**, 5378–5383 (2017).
16. B. Michon *et al.*, *Phys. Rev. X* **8**, 041010 (2018).
17. G. Grissonnanche *et al.*, *Nature* **571**, 376–380 (2019).
18. J. Zhang *et al.*, *Phys. Rev. B* **100**, 241114 (2019).
19. S. A. Hartnoll, *Nat. Phys.* **11**, 54–61 (2015).
20. S. A. Hartnoll, A. P. Mackenzie, *Rev. Mod. Phys.* **94**, 041002 (2022).

21. R. Mahajan, M. Barkeshli, S. A. Hartnoll, *Phys. Rev. B Condens. Matter Mater. Phys.* **88**, 125107 (2013).
22. T. Hartman, S. A. Hartnoll, R. Mahajan, *Phys. Rev. Lett.* **119**, 141601 (2017).
23. M. Ulaga, J. Mravlje, P. Prelovšek, J. Kokalj, *Phys. Rev. B* **106**, 245123 (2022).
24. D. P. Arovas, E. Berg, S. A. Kivelson, S. Raghu, *Annu. Rev. Condens. Matter Phys.* **13**, 239–274 (2022).
25. M. Qin, T. Schäfer, S. Andergassen, P. Corboz, E. Gull, *Annu. Rev. Condens. Matter Phys.* **13**, 275–302 (2022).
26. E. W. Huang, R. Sheppard, B. Moritz, T. P. Devereaux, *Science* **366**, 987–990 (2019).
27. P. T. Brown *et al*., *Science* **363**, 379–382 (2019).
28. M. A. Nichols *et al*., *Science* **363**, 383–387 (2019).
29. W. Xu, W. R. McGehee, W. N. Morong, B. DeMarco, *Nat. Commun.* **10**, 1588 (2019).
30. R. Blankenbecler, D. J. Scalapino, R. L. Sugar, *Phys. Rev. D Part. Fields* **24**, 2278–2286 (1981).
31. S. R. White *et al*., *Phys. Rev. B Condens. Matter* **40**, 506–516 (1989).
32. M. Jarrell, J. E. Gubernatis, *Phys. Rep.* **269**, 133–195 (1996).
33. O. Gunnarsson, M. W. Haverkort, G. Sangiovanni, *Phys. Rev. B Condens. Matter Mater. Phys.* **82**, 165125 (2010).
34. See supplementary materials.
35. W. O. Wang, J. K. Ding, B. Moritz, E. W. Huang, T. P. Devereaux, *Phys. Rev. B* **105**, L161103 (2022).
36. S. Mukerjee, V. Oganesyan, D. Huse, *Phys. Rev. B Condens. Matter Mater. Phys.* **73**, 035113 (2006).
37. R. E. Prange, L. P. Kadanoff, *Phys. Rev.* **134**, A566–A580 (1964).
38. C. H. Mousatov, S. A. Hartnoll, *NPJ Quantum Mater.* **6**, 81 (2021).
39. E. Tulipman, E. Berg, *NPJ Quantum Mater.* **8**, 66 (2023).
40. A. Lavasani, D. Bulmash, S. Das Sarma, *Phys. Rev. B* **99**, 085104 (2019).
41. W. O. Wang, Source code for "The Wiedemann-Franz law in doped Mott insulators without quasiparticles," Zenodo (2023). https://doi.org/10.5281/zenodo.7976147.
42. W. O. Wang, Data for "The Wiedemann-Franz law in doped Mott insulators without quasiparticles," Zenodo (2023). https://doi.org/10.5281/zenodo.7976153.

ACKNOWLEDGMENTS

We acknowledge helpful discussions with A. Auerbach, D. Belitz, E. Berg, S. A. Hartnoll, N. E. Hussey, S. A. Kivelson, P. A. Lee, R. T. Scalettar, Z. X. Shen, and E. Tulipman. **Funding:** This work was supported by the US Department of Energy (DOE), Office of Basic Energy Sciences, Division of Materials Sciences and Engineering. E.W.H. was supported by the Gordon and Betty Moore Foundation EPiQS Initiative through the grants GBMF 4305 and GBMF 8691. Y.S. was supported by the Gordon and Betty Moore Foundation's EPiQS Initiative through grants GBMF 4302 and GBMF 8686. Y.S.'s contribution to the work was done prior to joining AWS Center for Quantum Computing. Computational work was performed on the Sherlock cluster at Stanford University and on resources of the National Energy Research Scientific Computing Center, supported by the US DOE, Office of Science, under Contract no. DE-AC02-05CH11231. **Author contributions:** W.O.W. and T.P.D. conceived the study. W.O.W. performed numerical simulations and conducted data analysis and interpretation. J.K.D., Y.S., E.W.H., B.M., and T.P.D. assisted in data interpretation. W.O.W., B.M., and T.P.D. wrote the manuscript with input from all coauthors. **Competing interests:** The authors declare no competing interests. **Data and materials availability:** Code and data presented in this study are deposited in Zenodo (*41*, *42*).

SUPPLEMENTARY MATERIALS

science.org/doi/10.1126/science.ade3232
Materials and Methods
Supplementary Text
Figs. S1 to S15
References (*43*–*47*)

Submitted 8 August 2022; resubmitted 8 February 2023
Accepted 27 October 2023
10.1126/science.ade3232